

# Synthesis and magnetic properties of monodisperse magnetite nanocubes

Haitao Yang,<sup>1,a)</sup> Tomoyuki Ogawa,<sup>2</sup> Daiji Hasegawa,<sup>1</sup> and Migaku Takahashi<sup>1</sup>

<sup>1</sup>New Industry Creation Hatchery Center, Tohoku University, Aoba-yama 10, Sendai 980-8579, Japan

<sup>2</sup>Research Strategy and Support, Tohoku University, Aoba-yama 05, Sendai 980-8579, Japan

(Presented on 6 November 2007; received 11 September 2007; accepted 26 October 2007; published online 4 March 2008)

The monodisperse Fe<sub>3</sub>O<sub>4</sub> nanocubes with controllable sizes from 6.5 to 30.0 nm have been synthesized in one pot. The shape-induced texture of the self-assembled nanocube superlattices has been deposited onto substrates by a convective assembly technique. The cubelike shapes affect the crystalline orientation of individual particles within the self-assembled superlattices compared with the nanoparticles with an isotropic spherical shape. The nanocubes with a size less than 25 nm show a typical superparamagnetic behavior at room temperature. Comparison of the hysteresis loop at 5 K of cubes with different sizes reveals a size-dependent behavior of saturation magnetization and coercivity. © 2008 American Institute of Physics. [DOI: [10.1063/1.2833820](https://doi.org/10.1063/1.2833820)]

## INTRODUCTION

Enormous progress has been made in producing metal and semiconductor nanoparticles with various shapes such as rods, cubes, and prisms.<sup>1,2</sup> Different shapes of the particles can introduce electronic, optical, and magnetic properties that are different from those observed in their spherical counterparts.<sup>3</sup> Moreover, it is of great fundamental and practical interest to prepare self-assembled arrays by using different shapes as building blocks. Recently, various wet chemical approaches including hydrothermal synthesis and organic-phase synthesis have widely been used to prepare nonspherical nanoparticles since they provide great benefits in control of size, component, and dispersion.<sup>4,5</sup> However, there are several reports on the organic-phase synthesis of magnetic nonspherical nanoparticles, especially focused on FePt,<sup>6</sup> Co,<sup>7</sup> and MnFe<sub>2</sub>O<sub>4</sub> (Ref. 8) even though such monodisperse materials are of great importance in a variety of technological applications ranging from biomedical areas to magnetic data storage.

Magnetite (Fe<sub>3</sub>O<sub>4</sub>) is a common magnetic iron oxide and an important class of half-metallic materials.<sup>9</sup> Recent organic-phase synthesis studies on magnetite nanoparticles have mainly focused on size control and phase transfer. The monodisperse spherical magnetite nanoparticles with size varied from 4 to 20 nm have been synthesized by combining organic-phase reaction with seed-mediated growth.<sup>10</sup>

In this work, we present the one-pot synthesis of monodisperse Fe<sub>3</sub>O<sub>4</sub> nanocubes with controllable size from 6.0 to 30.0 nm by a modified polyol process in organic phase. A convective assembly by evaporation assisted withdrawal coating has been used to make superlattices of particles from dilute toluene/hexane suspensions. X-ray diffraction (XRD) of such a self-assembled texture of Fe<sub>3</sub>O<sub>4</sub> nanocubes on nonreflective Si substrate shows an intensified (220) peak. The hysteresis loops of Fe<sub>3</sub>O<sub>4</sub> nanocubes with different sizes at 300 and 5 K have been investigated.

## EXPERIMENTAL

In a typical synthesis of 15.0 nm Fe<sub>3</sub>O<sub>4</sub> nanocubes, a mixture of 0.5 mmol of Fe(acac)<sub>3</sub>, 4 mmol of 1,2-hexadecandiol, 8 mmol of oleic acid (OA), 2 mmol of oleyl amine, and 10 ml of benzyl ether was heated at 110 °C for 1 h with Ar flow. The temperature was then raised to 200 °C and kept at that temperature for 30 min. Under Ar blanketing, the mixture was heated to a reflux temperature of about 290 °C as a heating rate of 15 °C/min and kept refluxing for 1 h. The solution mixture was cooled down to room temperature, and the nanocubes were precipitated out by adding ethanol. The product was washed with ethanol and redissolved in the mixture of toluene and hexane.

Transmission electron microscopy (TEM, JEOL-3010 at 300 kV) was employed to determine the morphology, size, and size distribution of nanoparticles. Samples were formed by depositing toluene/hexane dispersion of particles on amorphous-carbon-coated copper grids in a convective assembly apparatus.<sup>11</sup> The sample was deposited on the nonreflective Si substrate (5 × 5 mm<sup>2</sup>) using the convective assembly technique for scanning electron microscopy (SEM, JEOL SM71010) and XRD (Rigaku 2200) measurement. The Fe mass in particles was firstly measured by our reported method<sup>12</sup> and the Fe<sub>3</sub>O<sub>4</sub> mass was then calculated via the stoichiometric ratio. Magnetic measurements were conducted using a Quantum Design MPMS-5 superconducting quantum interference device.

## RESULTS AND DISCUSSION

To achieve a shape-controlled synthesis, we modified slightly the synthesis procedure in Ref. 10. The molar ratio of OA to Fe(acac)<sub>3</sub> was increased to 4, while the molar ratio of oleyl amine and 1,2-hexadecandiol to Fe(acac)<sub>3</sub> was reduced. Such a modification based on that OA with a carboxylic group, -COOH, has a selective binding onto differing energy crystal facets together with a nonpolar tail group for steric hindering.<sup>13</sup> However, oleyl amine with a -NH<sub>2</sub> group has a weak and isotropic binding onto the surface of particles. The modified approach enables the control of the reactivity of the carboxylic group and as a result the nucleation

<sup>a)</sup>Author to whom correspondence should be addressed. Telephone: +81-22-795-7134. FAX: +81-22-263-9402. Electronic mail: [htyang@ecei.tohoku.ac.jp](mailto:htyang@ecei.tohoku.ac.jp).

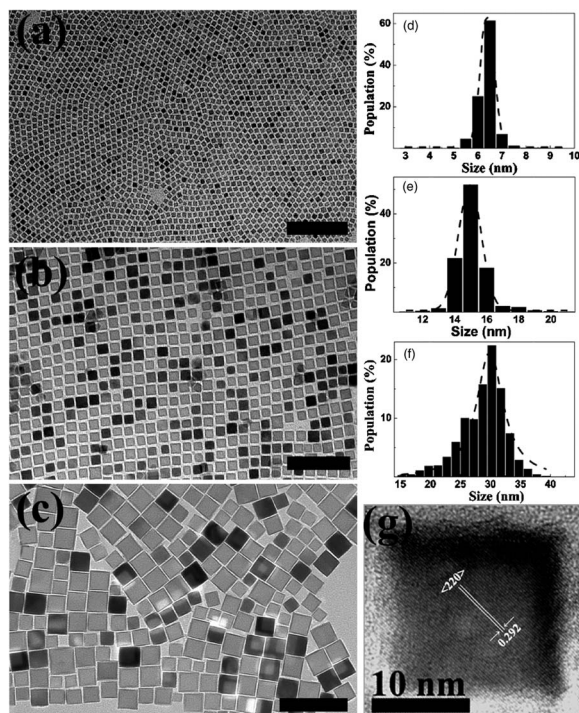


FIG. 1. TEM images of  $\text{Fe}_3\text{O}_4$  nanocubes with different sizes (a) 6.5 nm, (b) 15.0 nm, and (c) 30.0 nm and the corresponding size distribution histograms [(d)–(f)]. (g) HRTEM images of single 15.0 nm  $\text{Fe}_3\text{O}_4$  nanocubes with an interplanar spacing of 0.292 nm for the {220} plane.

and growth dynamics of the particles. By careful adjustment of the stabilizer molar amount as well as the reaction time we have obtained the size-controlled monodisperse magnetite nanocubes.

Figure 1 shows the TEM images of monodisperse  $\text{Fe}_3\text{O}_4$  nanocubes with different sizes from 6.5 to 30.0 nm. The IMAGEJ 1.3.2J software was used to determine the average particle size and the size distribution, analyzing at least 400 particles. The particle size was determined as the average of the major and minor axes of particles. The 15.0 nm cubes were synthesized with a heating rate of 15 °C/min and a reflux time of 1 h. Through quickly raising the reflux temperature from 200 °C as a rate of 35 °C/min and a short reflux time of 20 min, nanocubes with small sizes of less than 10 nm were obtained due to a relatively faster nucleation speed which favors the formation of more nuclei initially and thus a smaller size. To achieve nanocubes with big sizes, a slow nucleation speed adjusted by a heating rate of 5 °C/min and a long reflux time such as 3 h for the synthesis of 30 nm nanocubes were necessary. Such one-pot synthesis of monodisperse nanocubes with controlled size is facile only by adjusting the heating rate and the reflux time without a laborious multistep seed-mediated growth. With a size less than 15.0 nm, the nanocubes usually have a very narrow size distribution of less than 7% and the aspect ratios close to 1. Moreover, the nanocubes with small sizes well disperse in most of organic solvent such as hexane. However, with a size more than 25 nm, the size distribution increases greatly and the aspect ratios located between 1 and 1.5 together with a poor disperse in hexane. Typically, the 30 nm nanocubes have a size distribution of about 20%. Such a

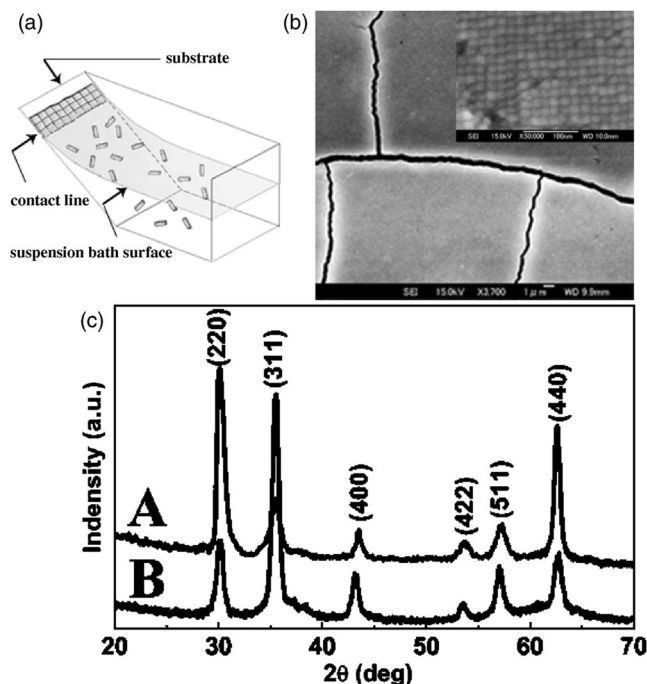


FIG. 2. (a) Diagram of the convective assembly process; (b) SEM image of  $\text{Fe}_3\text{O}_4$  nanocube superlattices on the Si substrate; the up-right inset is the enlarged partial image; (c) XRD patterns of nanocube (curve A) and nanoparticle (curve B) superlattices on nonreflective Si substrate.

phenomenon may be due to a pronounced Ostwald ripening happened in the synthesis of nanocubes with big sizes. Meanwhile, the strong magnetostatic interaction that existed in the nanocubes with big sizes lead to the aggregation of nanocubes resulted in depositing from suspensions. The high resolution TEM image of single 15.0 nm nanocubes is shown in Fig. 1(g). It shows that these nanocubes are single crystalline with an interplanar spacing of 0.292 nm for the {220} plane, which is consistent with the bulk values of magnetite with inverse spinel structure.

The convective assembly technique is illustrated in Fig. 2(a). The deposition was made directly onto an angled wall of the convective assembly apparatus. As the suspension evaporated slowly, the total bath level fell and caused the contact line to eventually sweep down the substrate and cover it with particles; the substrate, Si substrates, or TEM copper grids were effectively “withdrawn” relative to the bath. The suspension was diluted to between 0.002 and 0.05 vol %. Controlled evaporation of the carrier solvent from toluene/hexane dispersion of the particles led to  $\text{Fe}_3\text{O}_4$  nanocube superlattices. The SEM images of 15.0 nm  $\text{Fe}_3\text{O}_4$  nanocubes [as shown in Fig. 2(b)] reveal that most of nanocubes are the orientation ordering in the self-assembly superlattices though there are different defects such as cracks and holes. The 16.0 nm spherical nanoparticles synthesized by the method in Ref. 10 were also formed nanoparticle superlattices by the convective assembly technique. Figure 2(c) shows the XRD patterns of superlattice assembly from the 15.0 nm nanocubes and 16.0 nm spherical nanoparticles. The different shapes possessed by each group of the particles do affect the crystalline orientation of individual particles within the self-assembled superlattices. XRD of the self-assembled nanocubes on nonreflective Si substrate shows the intensified

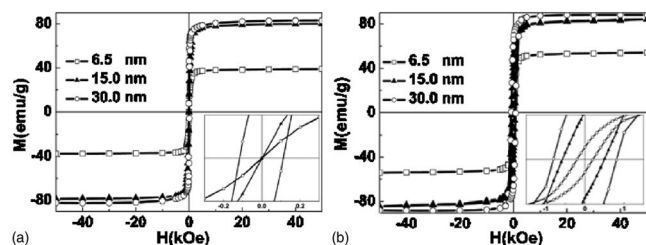


FIG. 3. Hysteresis loops at (a) 300 K and at (b) 5 K for  $\text{Fe}_3\text{O}_4$  nanocubes with different sizes of 6.5, 15.0, and 30.0 nm. The insert shows the enlarged partial hysteresis curves for  $\text{Fe}_3\text{O}_4$  nanocubes with different sizes.

(220) and (440) peaks in curve A of Fig. 2(c), which is markedly different from that of the self-assembled isotropic spherical particles with a strong (311) peak in curve B. The fact that the XRD of the nanocube assembly shows a strong (220) peak indicates that each of the cubelike particles in the superlattices has preferred crystal orientation with  $\{110\}$  planes parallel to the substrate. These demonstrate clearly that particle shape can indeed induce texture in a self-assembled particle superlattice.

Samples for the magnetic measurements were prepared by sealing the diluted magnetite nanocube solution in toluene/hexane (typically 0.1 vol %) into a quartz tube ( $\phi 5 \times 15 \text{ mm}^2$ ) in the glovebox with Araldite and the diamagnetic background from the quartz tube was subtracted. The hysteresis loops of the  $\text{Fe}_3\text{O}_4$  nanocubes with different sizes at 300 and 5 K are shown in Fig. 3. The saturation magnetizations ( $M_s$ ) at 300 K of  $\text{Fe}_3\text{O}_4$  nanocubes with sizes of 6.5, 15.0, and 30.0 nm were 39.5, 80.5, and 83.0 emu/g, respectively. The  $\text{Fe}_3\text{O}_4$  nanocubes with a size less than 25.0 nm possess typical superparamagnetic features at room temperature. However, the 30.0 nm  $\text{Fe}_3\text{O}_4$  nanocubes show a ferromagnetic behavior with a small coercivity ( $H_C$ ) of 100 Oe and a high  $M_s$  value close to that of the commercial magnetite powder (Aldrich catalog No. 31,006-9). For the nanocubes with small sizes, the loss of magnetization is possibly due to the contribution from small-size effect or spin canting at the outer surfactant layer of the particles. The field-dependent magnetizations at 5 K are presented in Fig. 3(b). The insert displays partial hysteresis curves for  $\text{Fe}_3\text{O}_4$  nanocubes with three different sizes at an enlarged scale of field strength for clearer viewing. All of the  $\text{Fe}_3\text{O}_4$  nanocubes with three different sizes show a size-dependent ferromagnetic behavior at low temperature. As for the saturation magnetization and coercivity, the trend for both of them is increased with increasing nanocube size. The  $M_s$  at 5 K of  $\text{Fe}_3\text{O}_4$  nanocubes with sizes of 6.5, 15.0, and 30.0 nm were 54.0, 84.0, and 88.0 emu/g, respectively, which are all a little higher than the corresponding values at 300 K. The  $H_C$  increased from 190 Oe for 6.5 nm to 500 Oe for 15.0 nm and 790 Oe for 30.0 nm  $\text{Fe}_3\text{O}_4$  nanocubes. The coercivity of magnetic nanocubes is surely related to the magnetic anisotropy, which originates from the spin-orbital coupling at crystal lattices. According to the Stoner-Wohlfarth single domain theory, the magnetocrystalline anisotropy energy  $E_A$  of single domain nanoparticles is approximated by  $E_A = KV \sin^2 \theta$ , where  $K$  is the magnetocrystalline anisotropy constant,  $V$  is the volume of nanoparticles, and  $\theta$  is the angle

between the easy axis of nanoparticles and the direction of field-induced magnetization. Both the magnetocrystalline anisotropy constant  $K$  and the volume of particles control the magnetic anisotropy. The single ion model has been successfully used in bulk magnetic materials to semiquantitatively evaluate the magnitude of anisotropy constant  $K$ .<sup>14,15</sup> The magnitude of  $K$  is closely related to the strength of spin-orbital coupling. Since the ligand field is weak in spinel ferrites, all cations assume high spin states. An  $\text{Fe}^{3+}$  cation with  $3d^5$  electron configuration usually has its orbital angular momentum quenched in a weak ligand field. Therefore, the contribution to the magnetic anisotropy should only come from  $\text{Fe}^{2+}$  cations in  $\text{Fe}_3\text{O}_4$ . Considering the ligand field at octahedral lattice sites, the  $3d^6$  electron configuration of the  $\text{Fe}^{2+}$  cation gives a ground energy state of  $^5T_{2g}$  under the  $O_h$  symmetry. However, this cubic symmetry is often lowered to a trigonal field in spinel due to the structural distortion from the Jahn-Teller effect. As a result, the triplet degenerated energy state of  $T_{2g}$  splits into two levels of  $E$  and  $B_2$  with  $B_2$  as the ground state. The orbital angular momentum in an  $\text{Fe}^{2+}$  cation with a  $B_2$  ground state is quenched and little spin-orbital coupling should be expected. So the volume of nanocubes is the dominant factor in the magnetic anisotropy of  $\text{Fe}_3\text{O}_4$  nanocubes. As a result, the coercivity of  $\text{Fe}_3\text{O}_4$  nanocubes is clearly increased with increasing nanocube size. In addition, the high coercivity of 30.0 nm  $\text{Fe}_3\text{O}_4$  nanocubes may also result from the shape anisotropy contribution since they have aspect ratios of more than 1.

In summary, we have developed a facile one-pot synthesis method of monodisperse size-controlled  $\text{Fe}_3\text{O}_4$  nanocubes in organic phase. Moreover, the shape-controlled synthesis and shape-induced texture of monodisperse  $\text{Fe}_3\text{O}_4$  nanocubes reveal that chemical process can be used to regulate the growth of a particle and control the crystal orientation of a particle in a superlattice assembly. A robust magnetic nanoparticle superlattice array with an aligned magnetic easy axis and controlled magnetic interactions between the neighboring particles may fabricate high-performance magnetic nanodevices in the future.

## ACKNOWLEDGMENTS

We thank Professor Shouheng Sun for helpful discussion and suggestion. This work is supported by the New Energy and Industrial Technology Development Organization (NEDO) of Japan and the Japan Society for the Promotion of Science (JSPS).

- <sup>1</sup>X. Peng *et al.*, *Nature (London)* **404**, 59 (2000).
- <sup>2</sup>T. S. Ahmadi *et al.*, *Science* **272**, 1924 (1996).
- <sup>3</sup>Y. Y. Yu *et al.*, *J. Phys. Chem. B* **101**, 6661 (1997).
- <sup>4</sup>J. Cheon *et al.*, *J. Am. Chem. Soc.* **126**, 1950 (2004).
- <sup>5</sup>V. F. Puentes *et al.*, *Angew. Chem., Int. Ed.* **45**, 3414 (2006).
- <sup>6</sup>O. Margeat *et al.*, *Phys. Rev. B* **75**, 134410 (2007).
- <sup>7</sup>V. F. Puentes *et al.*, *Science* **291**, 2115 (2001).
- <sup>8</sup>H. Zeng *et al.*, *J. Am. Chem. Soc.* **126**, 11458 (2004).
- <sup>9</sup>S. Soeya *et al.*, *Appl. Phys. Lett.* **80**, 823 (2002).
- <sup>10</sup>S. Sun and H. Zeng, *J. Am. Chem. Soc.* **124**, 8204 (2002).
- <sup>11</sup>J. A. Lee *et al.*, *Langmuir* **22**, 5217 (2006).
- <sup>12</sup>H. T. Yang *et al.*, *J. Appl. Phys.* **101**, 09J112 (2007).
- <sup>13</sup>P. D. Cozzoli *et al.*, *J. Am. Chem. Soc.* **125**, 14539 (2003).
- <sup>14</sup>K. Yosida and M. Tachiki, *Prog. Theor. Phys.* **17**, 331 (1957).
- <sup>15</sup>W. P. Wolf, *Phys. Rev.* **108**, 1152 (1957).